A numerical study exploring the effect of particle properties on the fluidization of adhesive particles

Robert Wilson, Daniele Dini, Berend van Wachem

January 7, 2016

Abstract

The effects of varying the elastic modulus, coefficient of restitution, and coefficient of friction of adhesive particles on fluidized bed dynamics have been investigated via numerical simulations. It is found that lower values of the elastic modulus and coefficient of restitution lead to a greater degree of particle clustering, and the formation of smaller bubbles. Coordination numbers are found to initially increase, and then fall, with increasing coefficient of friction, while bubble velocities follow the opposite trend. It is concluded that artificially reducing the elastic modulus of adhesive particles has a significant impact on the fluidization behaviour. The change in dynamics of the fluidized bed due to varying the coefficient of friction is more complex: particle clustering increases up to a point, beyond which clusters become increasingly rigid.

List of Figures

Introduction

Fluidized beds are a key element in many industrial processes. Strong interactions between the particulate and gas phase allow for efficient heat transfer and particle mixing, and provide a favourable environment for chemical reactions.[1] One of the most common applications is in fluidized bed reactors, used for large-scale reactions such as the Fluidic Catalytic Cracking (FCC) of fossil fuels, in which reactants are fed through a granular catalyst. Improving the performance of such reactors allows for faster and cheaper processes, and designing the system to optimise the reaction process is an ongoing area of work. This is a difficult task because of the complex nature of particle fluidization.

The behaviour of a fluidized bed is strongly dependent on the physical properties of both the solid and gas phase. For example, the dynamics are heavily influenced by the size of particles being fluidized. Powders were classified by Geldart[2] according to their fluidization characteristics. This classification scheme spans the range of particulate matter that may be fluidized, from the µm to the mm size range. Of great interest in the FCC industry are powders of diameter 50 µm to 100 µm,[3,4] which fall into group A (aeratable) in Geldart's classification scheme.

The influence of adhesive forces between particles is strongly dependent on particle size. Smaller particles have a higher surface area to volume ratio, and thus forces due to surface effects such as Van der Waals interactions and liquid bridging can become comparable in magnitude to other forces they experience. In particular, for dry powders of particles below $\sim 100\,\mu m$ Van der Waals forces become significant. Geldart group A powders are characterised by fluidization behaviour which arises from particle interactions. Phenomena such as homogeneous bed expansion before the onset of bubbling, and higher fluid velocities required for bubbling, are typical of such systems.

Understanding the dynamics of a fluidized bed is complicated by the fact that only macroscopic properties, such as the pressure drop, can be easily measured experimentally. Detailed information on the motion of individual particles within the bed is difficult to obtain. A number of particle tracking methods exist, *e.g.* the use of radioactive tracer particles or optical fibre probes,[4] but they typically involve influencing the system in some way. For example, radioactive tracer particles will exhibit

different properties to the rest of the powder, and therefore not necessarily give representative results. For this reason, computer simulation has become a valuable tool for gaining insight into the small-scale dynamics of fluidization.

Multiphase flows are commonly simulated by treating the particles as either a continuous Eulerian phase, or as discrete Lagrangian elements.[5,6] A Eulerian approach is capable of simulating a number of particles comparable to that of typical systems, but at the expense of information on individual particle trajectories. It is also worth noting that only average particle behaviour is represented, and that more complex particle interactions such as adhesion are significantly more difficult to implement in a Eulerian framework.[7] On the other hand a Lagrangian model, usually implemented using the Discrete Element Model (DEM),[8] accurately describes the motion of each particle. As the timescale associated with particle collisions is much smaller than that upon which the fluid phase evolves, DEM simulations can be computationally expensive. Because of this, the number of particles which can feasibly be simulated ($< 10^7$) is much smaller than usually occurs in typical applications ($> 10^8$).

Within the DEM framework there are two common approaches to describing collisions between particles. In the soft-sphere approach, originally proposed by Cundall and Strack,[8] particles are allowed to overlap, and forces describing the collision are calculated based on the magnitude of this overlap. A large number of collision models exist but can be broadly categorised based on whether the contact force is linear[8] or Hertzian.[9] For such a collision it is necessary that the timestep of integration is sufficiently small that the evolution of inter-particle forces is adequately resolved. Alternatively, a hard-sphere collision model[10] can be used, in which case collisions are assumed to be instantaneous and binary. Due to the binary nature of collisions, hard-sphere models are unsuitable for dense systems of particles, where contact may be maintained between multiple particles for protracted time periods. As this is frequently the case in a fluidized bed, a soft-sphere method has been utilized in the present work.

There have been a number of DEM studies of the effects of varying the physical particle parameters on the fluidization of group A particles.[11–14] Moreno-Atanasio and Ghadiri[11] consider the fluidization

of soft and hard particles with strong and weak adhesive forces, and conclude that as adhesive forces become stronger the contact stiffness has a large influence on the fluidization behaviour. Kobayashi *et al.*[13] reach the same conclusions, and propose a new model for adhesion, which is demonstrated to somewhat counteract the change in contact stiffness. Hou *et al.*[12] investigate the effect of particle size, finding a number of novel differences between the various flow regimes, and between group A and B powders. Yang *et al.*[14] simulate powders which experience adhesion to varying degrees, and characterise the fluidization behaviour at various velocities.

In the present work we investigate the effects of varying the elastic modulus, coefficient of restitution, and coefficient of friction on the fluidization of adhesive powders. The elastic modulus is of interest because in DEM simulations it is nearly always reduced compared to the elastic modulus of particles found in real powders. Dissipation in the system, parametrised by the coefficient of restitution, has a large impact on the dynamics of a fluidized bed. Friction plays an important role when considering adhesive particles because two particles in contact and at equilibrium will have a finite contact area between them. In order for these particles to slip over one another a critical tangential force must be applied, the magnitude of which will depend on the strength of adhesion and coefficient of friction. This study differs from much previous work in its use of non-linear contact forces, and a 3D domain, the advantages of which are discussed further in the 'Numerical model' section. The effects of the coefficients of friction and restitution on Geldart A powders have not been previously investigated. Additionally the properties of bubbles in the bubbling regime of the bed have been investigated, revealing further details on the dynamics of fluidization.

The numerical model used in this work is stated and discussed in the 'Numerical model' section. Effects of adhesion on the dynamics of individual collisions are further investigated in the 'Individual contacts' section. Results are presented and discussed in the 'Results and discussion' section, and conclusions drawn in the 'Conclusions' section.

Numerical model

Particle modelling

Equations of motion

Particles are modelled by integrating Newton's second law. A particle of mass m and moment of inertia I at position r may experience forces from three origins: gravity, $m\vec{\boldsymbol{g}}$, particle contacts, $\vec{\boldsymbol{f}}_c$, and fluid interactions, $\vec{\boldsymbol{f}}_f$. Additionally the angular velocity, $\vec{\boldsymbol{\omega}}$, may be changed by torques associated with contacts, $\vec{\boldsymbol{T}}_c$. Thus each particle obeys the following equations of motion:

$$m\ddot{\vec{\boldsymbol{r}}} = m\vec{\boldsymbol{g}} + \vec{\boldsymbol{f}}_c + \vec{\boldsymbol{f}}_f, \tag{1}$$

$$I\dot{\vec{\boldsymbol{\omega}}} = \vec{\boldsymbol{T}}_c. \tag{2}$$

These equations are solved using a Verlet integration scheme.

Contact forces

There are a number of approaches which may be used to describe soft-sphere particle-particle interactions in DEM. The original model, proposed by Cundall and Strack,[8] prescribed a damped spring normal contact force, and is still widely used today. This approach has a number of advantages: it is easy to implement and fast to compute, and the duration of each collision can be related to the period of the equivalent harmonic oscillator. A suitable timestep for the particle phase can therefore be calculated based on this period in order to resolve each collision with sufficient accuracy. Linear forces have the significant disadvantage that they do not provide a physically accurate description of the force between two particles. The contact stiffness does not correspond to any measurable physical quantity, and is frequently calibrated such that on average the correct elastic energy is stored during a collision.

It is well known that the force transmitted between two elastic spheres is related to the overlap,

δ, by the Hertzian relationship,[9] proportional to $\delta^{3/2}$. This relationship is used by a number of DEM force models,[15,16] which differ in their treatment of dissipative and tangential forces. Unlike the linear model, the mathematical expression of the Hertzian force depends on the physical properties of the particle. While the non-linear force does take longer to calculate numerically, the number of collisions increases linearly with the number of particles, N, so it is unlikely to significantly slow down a simulation compared to *e.g.* calculating which particles are colliding, which scales at best as $N\log(N)$. Selecting an optimal timestep is not as simple with the Hertzian model as it is in the linear case. However, by considering the energy stored in collisions it is still possible to calculate a timestep such that every collision will be sufficiently resolved.[17] The method by which this is achieved is outlined in the 'Timestep' section.

In this study, the repulsive component of the normal force between particles is described using the model proposed by Tsuji *et al.*[15] This model uses a Hertzian contact force, with a dissipative component tuned such that the coefficient of restitution is correct. For a collision with overlap δ_n, relative particle velocity $\vec{\boldsymbol{v}}$, and normal $\hat{\boldsymbol{n}}$, the normal force has the form

$$\vec{\boldsymbol{f}}_n = (K_n\delta_n^{3/2} - \eta_n\vec{\boldsymbol{v}}\cdot\hat{\boldsymbol{n}})\hat{\boldsymbol{n}}, \tag{3}$$

where K_n and η_n are constants which depend upon the physical properties of the particles. For a collision between two dissimilar particles, denoted by subscripts 1 and 2, the reduced radius, $r^* = \frac{r_1 r_2}{r_1+r_2}$, and reduced elastic modulus $E^* = \frac{E_1 E_2}{E_1(1-\nu_2^2)+E_2(1-\nu_1^2)}$ are used.

$$K_n = \frac{4r^*}{3E^*}, \tag{4}$$

$$\eta_n = \alpha(mK_n)^{1/2}\delta_n^{1/4}. \tag{5}$$

α is a constant that may be used to determine the coefficient of restitution independently of the other parameters.

Adhesive forces

Adhesive forces between particles have been a subject of study since the initial investigations of Bradley.[18] There are several possible adhesion mechanisms, *e.g.* electrostatic attraction and liquid bridging, however in the present study we are interested only in Van der Waals forces. Adhesion between elastic spheres is well understood, and usually described using the DMT[19] or JKR[20] models. The discrepancy between the behaviour predicted by these two models was explained by Maugis,[21] who recognised that the DMT model is applicable in the case where adhesive forces are weak and particles are hard, whereas the JKR approach accurately describes soft, sticky particles. This result was been confirmed by numerical calculations of normal contact between adhesive elastic spheres.[22]

Particles are frequently characterised by the Tabor parameter,[23] μ; a dimensionless number which gives a measure of the extent to which adhesive forces are capable of deforming the particle. Adhesive forces are characterised by the work of adhesion, $\Delta\gamma$; the energy per unit area required to pull two infinite, flat surfaces apart, and the equilibrium distance, ε.

$$\mu = \left(\frac{r^* \Delta\gamma^2}{E^{*2} \varepsilon^3} \right)^{1/3} \tag{6}$$

This parameter is useful for characterising the adhesive behaviour of particles as either the DMT ($\mu < 1$) or JKR ($\mu > 1$) regime.

The powders of interest in the present study – typically consisting of materials such as zeolite – are in the regime described by the DMT model. In the initial publication of the DMT model[19] a number of formulations for the force between two particles were given, however it was later shown[24] that only one of these was correct. By numerically integrating equation 16 in[24] we obtain the DMT adhesion force, shown in figure 1. When this is added to the repulsive Hertzian expression, the total static normal force is obtained. This result is shown to be very similar to the total force obtained by adding a constant value of $2\pi R\Delta\gamma$ to the Hertzian expression.

The pull-off force is defined as the maximum force required to pull two particles out of contact.

Both DMT and JKR models tend to predict a higher pull-off force than is observed experimentally.[25] This is primarily due to the roughness of real surfaces, which leads to a much smaller contact area than for a smooth surface.[26] For surfaces in the DMT regime this effect is particularly prominent; the deformation of the highest asperities provide a large repulsive force, while the rest of the surface is at too great a separation to experience significant attraction. Because of this, the standard DMT model does not provide an accurate representation of the force between surfaces. However, there is not currently a model for the contact force between rough surfaces which is both accurate and sufficiently fast to be used in a DEM simulation.

In this study adhesion is described using a constant force of

$$\vec{\boldsymbol{f}}_{adh} = -2\pi r^* \Delta\gamma \hat{\boldsymbol{n}}, \tag{7}$$

which opposes the Tsuji contact force. This is justified because of the inadequacies of more complex models to describe realistic surfaces, and the small difference between the DMT model and a constant adhesive component demonstrated in figure 1. The force is very similar in magnitude to the DMT force with low μ and the same $\Delta\gamma$, but significantly faster to compute. In addition, the value of $\Delta\gamma$ is calculated from the measurements of adhesive forces between zeolite particles,[27] so that it will better represent the adhesion seen in a real system.

The strength of adhesive inter-particle forces is frequently characterised by the Bond number, B; the ratio of the adhesive and gravitational forces acting on a particle. It is expected that particles with a low Bond number (< 1) will exhibit Geldart B type behaviour, whereas when $B \gtrsim 1$ adhesive forces have more influence on the bed behaviour and the transition to Geldart A type behaviour will be observed. Particles of diameter d =60 µm, density ρ =2200 kg m^{-3}, and work of adhesion $\Delta\gamma$ =5×10^{-4} J m^{-2} have a bond number of $B \approx 2$.

The total contact force is then given by a combination of the Tsuji and adhesive components:

$$\vec{\boldsymbol{f}}_c = \vec{\boldsymbol{f}}_n + \vec{\boldsymbol{f}}_{adh}. \tag{8}$$

Tangential forces

The full effect of adhesion on the friction of a contact is complex, as there are typically regions of positive and negative pressure, which are not taken into account by most friction models. However, frictional forces can be related to the contact area.[20,28] For two adhesive particles in contact there is a finite contact area at zero normal force. Because of this, the normal force considered when calculating the slip/stick behaviour is not the total normal force experienced by the particle. Instead, only the Tsuji model component of the normal force is considered, without the adhesive term.

Tangential forces, $\vec{\boldsymbol{f}}_t$, are described using a linear spring and dashpot, with a coulomb type mechanism for sliding.[29] Relevant parameters are the tangential spring constant, k_t, tangential displacement, $\vec{\boldsymbol{\delta}}_t$, slip velocity, $\vec{\boldsymbol{v}}_s$, and coefficient of friction, μ_f.

$$\vec{\boldsymbol{f}}_t = \begin{cases} -k_t\vec{\boldsymbol{\delta}}_t - \eta\vec{\boldsymbol{v}}_s & \text{if } |\vec{\boldsymbol{f}}_t| < \mu_f|\vec{\boldsymbol{f}}_n|, \\ -\mu_f|\vec{\boldsymbol{f}}_n|\hat{\boldsymbol{t}} & \text{otherwise,} \end{cases} \tag{9}$$

(10)

where $\hat{\boldsymbol{t}}$ opposes the direction of sliding. Particles may rotate during a collision, and it is necessary to remap the tangential force such that it lies in the plane defined by the collision normal, $\hat{\boldsymbol{n}}$. Relevant rotations can be described by vectors perpendicular to $\vec{\boldsymbol{f}}_t$, and decomposed into those either parallel or perpendicular to $\hat{\boldsymbol{n}}$.

The correction is made in two steps: first the rotation from the old collision normal $\hat{\boldsymbol{n}}^{old}$ to $\hat{\boldsymbol{n}}$ is expressed as

$$\vec{\boldsymbol{\delta\theta}} = \hat{\boldsymbol{n}}^{old} \times \hat{\boldsymbol{n}}. \tag{11}$$

Assuming that the small angle approximation is valid, the tangential force vector can then be rotated such that it is perpendicular to $\hat{\boldsymbol{n}}$.

$$\vec{\boldsymbol{f}}_t' = \vec{\boldsymbol{f}}_t^{old} + \vec{\boldsymbol{\delta\theta}} \times \vec{\boldsymbol{f}}_t^{old} \tag{12}$$

Step two is to make a rotation parallel to $\hat{\boldsymbol{n}}$. The angular velocity at which the collision is rotating is calculated from the angular velocities of the two particles, denoted $\vec{\omega}_1$ and $\vec{\omega}_2$.

$$\vec{\omega}_{col} = \left[\frac{1}{2}\left(\vec{\omega}_1 + \vec{\omega}_2\right) \cdot \hat{\boldsymbol{n}}\right] \hat{\boldsymbol{n}} \tag{13}$$

Then the final remapped tangential force is given by a similar procedure to equation 12, with the rotation vector given by $\Delta t \vec{\omega}_{col}$,

$$\vec{\boldsymbol{f}}_t = \vec{\boldsymbol{f}}_t' + \Delta t \vec{\omega}_{col} \times \vec{\boldsymbol{f}}_t'. \tag{14}$$

It is worth noting that this method requires that, from one timestep to the next, both the angle by which the collision has rotated, and the angle rotated by each particle, are small. This is not only because of the approximation used in expressions 12 and 14, but also because rotations around perpendicular axes can only be considered as commutative in the limit of small angles. While equations 12 and 14 could be easily rewritten to account for large rotational velocities, the combination of the two rotations would be less simple. It has been observed that, provided the timestep is sufficiently small to resolve the normal component of the collision, this approximation is valid.

Fluid interactions

The full interaction between a sphere and a non-uniform fluid flow is described by the BBO (Basset, Boussinesq and Oseen) equation, a derivation of which has been presented by Maxey.[30] In a gas-fluidized bed it is always the case that the density of the solid phase, ρ_s, is much greater than that of the fluid phase, ρ_f. Because of this, the dominant forces acting on a particle due to the fluid phase are the drag force, $\vec{\boldsymbol{f}}_d$, and pressure gradients, $\vec{\boldsymbol{f}}_p$.

The drag force depends on the difference between the velocity of a particle, $\vec{\boldsymbol{v}}_p$ and that of the surrounding fluid, $\vec{\boldsymbol{v}}_f$. There are a number of models that are frequently used to model this phenomenon. Popular expressions for the drag force include those of Wen and Yu,[31] and Gidaspow.[32] Gidaspow's method involves using the Ergun correlation[33] when the concentration of solid phase is high, and the

Wen and Yu model in more dilute regions. In the present work, the expression of Wen and Yu is used, as it has been found in previous studies[34] to perform better than that of Gidaspow in the context of a fluidized bed. This can be attributed in part to the absence of a discontinuity in the drag coefficient, which is a feature of Gidaspow's model. For a particle of volume V_p and diameter d_p, with a local fluid volume fraction ε_f, the drag force can be expressed as

$$\vec{\boldsymbol{f}}_d = \beta \frac{V_p}{(1-\varepsilon_f)} \left(\vec{\boldsymbol{v}}_f - \vec{\boldsymbol{v}}_p\right). \tag{15}$$

The momentum transfer coefficient, β, is defined to be[31]

$$\beta = C_d \frac{3\varepsilon_f(1-\varepsilon_f)\rho_f|\vec{\boldsymbol{v}}_f - \vec{\boldsymbol{v}}_p|}{4d_p}\varepsilon_f^{-2.65}, \tag{16}$$

where the drag coefficient, C_d, is determined by the particle Reynolds number, Re:

$$C_d = \begin{cases} \frac{24}{Re\,\varepsilon_f}\left(1 + 0.15(\varepsilon_f\, Re)^{0.687}\right) & \text{if } \varepsilon_f\, Re < 1000, \\ 0.44 & \text{if } \varepsilon_f\, Re > 1000. \end{cases} \tag{17}$$

Forces acting due to gradients in the fluid pressure field, P_f, have the form

$$\vec{\boldsymbol{f}}_p = V_p \nabla P_f. \tag{18}$$

Consequences of this equation are that particles will experience a force both because of pressure fluctuations in the fluid, *e.g.* in the vicinity of a bubble in a fluidized bed, and also the pressure gradient due to gravity.

Fluid modelling

The motion of the gas phase is calculated by numerically solving the locally averaged equations of motion.[35] For a gas of density ρ_f, velocity $\vec{\boldsymbol{v_f}}$, and volume fraction ε_f, conservation of mass is ensured

by the continuity equation,

$$\frac{\partial(\varepsilon_f \rho_f)}{\partial t} + \frac{\partial(\varepsilon_f v_{f,i})}{\partial x_i} = 0. \tag{19}$$

For momentum conservation it is necessary to take into account the effect of gravity, $\vec{g}$, and the interaction with the particle phase. Particles are treated as point sources of momentum. The magnitude of the momentum imparted by each particle is equal and opposite to that imparted by the fluid to that particle, as expressed in equation 15. With the volume and velocity of particle k denoted by V_k and v_k respectively, the locally averaged momentum equation can be expressed as

$$\frac{\partial(\varepsilon_f \rho_f v_{f,j})}{\partial t} + \frac{\partial(\epsilon_f \rho_f v_{f,i} v_{f,j})}{\partial x_i} = -\varepsilon_f \frac{\partial P}{\partial x_j} - \varepsilon_f \frac{\partial \tau_{ij}}{\partial x_i} + \varepsilon_f \rho_f g_j - \sum_k \beta \frac{V_k}{(1-\varepsilon_f)} \left(v_{f,j} - v_{k,j}\right). \tag{20}$$

In equations 19 and 20 vector components are represented by indices and repeated indices are summed over. These equations are discretized and solved using the finite volume method.

Simulation conditions

Physical Parameters

Unless otherwise stated, all simulations were carried out with physical parameters as stated in table 1. Particle properties correspond to a zeolite powder,[36] with the exception of the elastic modulus, which is varied over the range which can be feasibly simulated using DEM – see the sections 'Individual contacts' and 'The elastic modulus'. Fluid properties are those of hot air.

The simulation domain has a z dimension of only ~ 6 particle diameters, compared to ~ 60 and ~ 150 in the y and x dimensions respectively. In the z direction there are periodic boundary conditions for the particle phase. This allows significantly fewer particles to be simulated than would be required in *e.g.* a domain with a z dimension equal to the y dimension. A number of studies[12,37] have found that such a system gives results that are more physical than a 2D simulation, particularly in cases involving a distribution of particle sizes.

While better than a 2D DEM simulation, it is not expected that such a thin system will replicate the

results of a fully 3D system. The ways that this influences the results may be inferred from comparisons of 2D and 3D Euler-Euler systems.[38] It is observed that while general trends are observable in 2D and 3D simulations, 3D systems exhibit more realistic physical behaviour, in particular bubble radii are noted to be smaller in 2D systems. This is unsurprising, as bubbles in a thin, periodic system essentially represent infinite tubes. As a result, for many measurable properties it is not possible to make quantitative comparisons between thin systems and experimental data.

Timestep

Particle timesteps were calculated adaptively,[17] using the following method. For a particle collision with an overlap of δ, the elastic energy stored in the Hertzian spring can be easily calculated. The equivalent linear spring – that which gives the same energy at the same δ – is then found. A sensible timestep for the collision at that point can be calculated as some fraction of the time period of the equivalent linear spring, sufficiently small as to ensure that the collision is well resolved. Thus as δ increases, the appropriate timestep is reduced accordingly. After calculating the necessary timestep for each collision, the particle timestep for the simulation can be set equal to the smallest of them. By repeating this process regularly, it is ensured that the timestep is always at an optimal value. Typical timesteps ranged from $\sim 2.5 \times 10^{-7}$ s for an elastic modulus of 3.16×10^{6} Pa to $\sim 4 \times 10^{-8}$ s for $E = 3.16 \times 10^{8}$ Pa.

Fluid Phase

In a simulation such as this it is necessary for the fluid mesh to be sufficiently finely resolved to describe phenomena of interest, in this case bubbles propogating through the bed. However as the fluid equations of motion rely on the average volume fraction of a dispersed particulate phase, the accuracy of the flow field does not increase below some threshold cell size. An optimal cell size is therefore sufficiently small to describe bubbles in the system, but not so small that solving the fluid equations incurs extra computational cost with no increase in accuracy. Cubic fluid cells of side length

0.18×10^{-3} m were chosen for this study, making a domain of $2 \times 20 \times 50$ cells. A fluid timestep of 2×10^{-4} s was found to be optimal.

Boundary conditions for the velocity, $\vec{\boldsymbol{v_f}}$, of the fluid phase were chosen as follows. The faces in the y plane had constraints of $\vec{\boldsymbol{v}} = \vec{\mathbf{0}}$, leading to a parabolic velocity profile. In the x plane, conditions of $v_x = 0$ and $\frac{d}{dx}v_y = \frac{d}{dx}v_z = 0$ ensured that there was no flow in that direction. The inlet had a constant velocity, v_{inlet}, scaled by the volume fraction, ε, in each cell: $v_z = v_{\text{inlet}}/\varepsilon$. At the outlet the velocity gradient was set to zero, $\nabla\vec{\boldsymbol{v}} = \vec{\mathbf{0}}$, and the pressure set to zero. The pressure at every other boundary was extrapolated from the flow field.

A snapshot of a typical simulation is shown in figure 2. In this case particle properties exactly match those in table 1.

Individual contacts

It is common practice in DEM simulations to reduce the elastic modulus – or contact stiffness in the case of a linear contact model – of particles by several orders of magnitude compared to the material being simulated. This allows a significantly larger timestep to be used for the particulate phase, and therefore reduces the computational cost of simulations. It has been shown in a previous study[39] that in a fluidized bed of non-adhesive particles the contact stiffness does not significantly effect the dynamics of the system, allowing the simulation of soft particles to represent much harder materials.

In the case of adhesive particles, a change in elastic modulus affects more than just the duration of collisions. While in a non-adhesive system the rebound velocity is determined purely by the dissipative term, frequently parametrised using a coefficient of restitution, in the adhesive case the situation is more complex. When adhesive particles collide at sufficiently low normal velocities they stick together. A critical velocity, v_c, can be defined, below which two particles will stick together and above which they bounce. The overlap between particles during two collisions, one with an incident velocity just below v_c, and the other just above, can be seen in figure 3. Whether or not particles have enough kinetic energy to bounce off one another will determine the degree to which clusters form, and can

therefore greatly influence the behaviour of a system of dynamic particles.

Adhesion was implemented using a force that is independent of the particles' elastic properties. It is therefore unsurprising that for particles with a lower elastic modulus, if other properties are kept constant, the adhesive force will lead to a larger overlap and there will be a greater potential for dissipative losses. If elasticity is taken into account, as in the JKR model for instance, a reduction in elastic modulus tends to *increase* the total adhesive energy, which would further contribute to this effect. The critical velocity was calculated numerically for a range of elastic moduli, and is plotted in figure 4. The increase in v_c with lower elastic modulus is attributed to the increased dissipative losses, as more kinetic energy is required for particles to bounce off one another. Consequently, simulating soft adhesive particles to allow for larger timesteps may lead to particles which are more inclined to stick together, and therefore even greater energy dissipation via collisions.

The stick/bounce behaviour of adhesive particles also has ramifications when considering the coefficient of restitution. Figure 5 demonstrates the problem with defining a coefficient of restitution in this case. Whereas for non-adhesive particles there is a linear relationship between initial and final velocity, the adhesive case can be split into three regions. For low velocities the final velocity is zero as the particles stick together. Just above the critical velocity the final velocity rapidly increases in a non-linear fashion. At higher initial velocities the final velocity increases approximately linearly, and has a gradient matching the coefficient of restitution in the non-adhesive case, however there is an offset corresponding to energy lost due to adhesion.

Relatively small changes to the dynamics of individual particle collisions can lead to very different behaviour in a system of many such particles. In section the following section we investigate the effects of changing the elastic modulus in a fluidized bed.

Results and discussion

The elastic modulus

Fluidized beds of adhesive particles were simulated, with the elastic modulus varied from 3.16×10^6 Pa to 3.16×10^8 Pa. This range notably falls short of the true elastic modulus of zeolite, ~ 78 GPa. Indeed it is rarely feasible to simulate a material with its true elastic modulus using DEM; it was found that even for a relatively small system, values of $E \gtrsim 10^9$ carried a significant computational cost.

The distribution of particle coordination numbers – the number of inter-particle contacts – gives an indication of the tendency for cluster formation in a system. Figure 6a shows the probability distributions of coordination numbers for three elastic moduli. This graph shows a transition from a state where no bubbles propogate, at $E = 3.16 \times 10^6$ Pa, to a freely bubbling bed. This is in contrast to the non-adhesive case, in which bubbles propogate at all elastic moduli. In figure 6b the average coordination numbers for adhesive and non-adhesive particles are shown. The average number of contacts per particle decreases substantially with increasing elastic modulus, for both adhesive and non-adhesive particles, implying that softer particles are more inclined to form clusters. Adhesive particles both exhibit higher average coordination numbers, as might be expected, and a greater increase in average coordination number as E is reduced. This is likely a result of the increase in the critical velocity, discussed in the 'Individual contacts' section, as harder particles require less energy to bounce off one another. The effects that this may have on the propagation of bubbles through the bed are of particular interest.

Bubbles have been characterised by their size and velocity. It is observed that for a small bed such as those being simulated, bubbles tend to fall into two categories: large, fast moving bubbles near the centre of the bed, and smaller, slow bubbles creeping up the walls. In larger beds, such as those used in industry, it is likely that bubbles would be predominantly of the first kind, as the boundary layer near the walls will exert far less influence over the system. Because of this we consider only the properties of the freely moving bubbles near the centre.

Figures 7 and 8 illustrate the effects of elastic modulus on the volume and velocity of bubbles respectively. Figure 7b demonstrates that for adhesive particles an increase in elastic modulus leads to a larger average bubble size. This is likely because more energy is dissipated while pulling softer particles out of contact, and it is therefore more difficult to expand bed of such particles to form a bubble. The PDF for bubble volumes reveals a very different distribution for an elastic modulus of 3.16×10^6 Pa than for higher values. While for elastic moduli of 3.16×10^7 Pa and 3.16×10^8 Pa bubble volumes follow a broad distribution of similar shape, the distribution at low elastic modulus consists exclusively of very small bubbles. The reason for this is revealed by the properties of the distribution of void velocities, figures 8a and 8b, in which it can be seen that for the lowest elastic modulus the voids are stationary. This is confirmed by looking at the bed dynamics: the 'bubbles' in the low elastic modulus case are in fact static voids in the particle bed. It is inferred that at such a low elastic modulus adhesive and dissipative forces dominate, and a higher pressure is needed to overcome them, increasing the minimum bubbling velocity. For the higher elastic moduli the average bubble velocity, and PDFs of bubble velocities, are similar, despite the apparent variation in average bubble sizes.

In contrast, the non-adhesive case exhibits no obvious trends in bubble size or volume as a function of elastic modulus. This lends support to the notion that for non-adhesive particles it is possible to artificially reduce the elastic modulus without significantly changing the system dynamics.

The pressure difference between the top and bottom of a fluidized bed gives useful information on the behaviour of the bed. How this pressure changes with inlet velocity is shown in figure 9 for three of the elastic moduli which were investigated. In these simulations a smaller system of 19244 particles was investigated, as a greater number of timesteps were required to adequately cover the relevant range of inlet velocities and it became necessary to reduce computational cost. As the fluid velocity is increased from zero up to and beyond the fluidization velocity, v_{mf}, the system passes through a number of distinct regimes. Those which can be identified in figure 9 are as follows:

$v < v_{mf}$**:** Pressure increases linearly with inlet velocity

$v_{mf} < v < v_{mb}$: The bed expands as particles start to move, some slow wavelike bubbles propagate leading to pressure fluctuations

$v > v_{mb}$: Bubbles form freely – pressure fluctuates rapidly

For an elastic modulus of 3.16×10^6 Pa the transition to a freely bubbling bed occurs at a relatively high velocity of approximately $17.5 \times 10^{-3}\,\mathrm{m\,s^{-1}}$. On the other hand, for $E = 3.16 \times 10^8$ Pa bubbling occurs at a lower velocity, and the system does not spend long in the expanded bed regime, transitioning to a freely bubbling bed at around $7.5 \times 10^{-3}\,\mathrm{m\,s^{-1}}$. If the system is given longer to equilibrate while in the regime of $v_{mf} < v < v_{mb}$, it settles to a static expanded bed, as is the case in figures 6 to 8 for the E =3.16×10^6 Pa case.

The increased computational cost of using larger elastic moduli leads to longer simulation times. This results in simulations of harder particles taking longer than the equivalent simulation for softer particles. The time taken to simulate a fluidized bed for 1 s using each of the elastic moduli investigated is shown in figure 10. While the exact times will depend on the computer which is running the simulation, in most cases the general trend will not.

It can be clearly seen on figure 10 that the time required to run a simulation increases dramatically as the elastic modulus is increased. Real materials typically exhibit an elastic modulus of $> 10^{10}$ GPa, however such high values would result in a prohibitively small particle timestep.

The coefficient of restitution

The dynamics of a system of adhesive particles depend strongly on both the elastic properties and the dissipation in the system. When the normal force contains an adhesive component, what is included in Tsuji's model as the 'coefficient of restitution' no longer represents the ratio of initial to final velocities, as discussed in the 'Individual contacts' section. This is the parameter which may be used to vary dissipation, and will continue to be referred to as the coefficient of restitution (e), however it must be noted that this is no longer an accurate description. Varying the coefficient of restitution has a somewhat similar effect to changing the elastic modulus. In the case of the coordination number, an

increase in e corresponds to a lower critical bounce velocity and therefore less clustering of particles. This can be seen in figure 11.

The coefficient of friction

Tangential forces between particles also play a role in determining the behaviour of a fluidized bed. For adhesive particles in particular the magnitude of μ is important, as there will be a significantly larger contact area associated with most collisions than in the non-adhesive case. When particles cluster together, the extent to which they can be rearranged is determined in part by the ease at which they can slip over one another. Additionally, whether two particles colliding at an oblique angle stick or bounce is determined in part by how much tangential velocity is dissipated.

Simulations were performed in which μ was varied, while other properties were kept constant at the values stated in table 1. Figure 12 shows that for low values of μ the behaviour is as might be expected, *i.e.* as the friction increases particles are likely to form larger clusters due to the increased dissipation. However, as μ is increased above 0.15 the average coordination number falls again. This somewhat unintuitive result is attributed to the increasing rigidity of clusters as friction starts to dominate; the particles become unable to slide at all, and therefore will not rearrange within a cluster.

In order for slip at the contact to occur, a critical tangential force of $F_\mu = \mu F_n$ must be applied. For a contact between two adhesive particles under no external normal loading, the value of F_n at equilibrium is the pull-off force, $F_{\text{pull-off}}$. Plotting the ratio of tangential force to F_μ for each particle in a system gives a good indication of whether particles are able to freely slip. The distribution of this ratio for a timestep of the simulation is shown in figure 13 for three values of μ. These graphs support the argument that at high μ clusters become increasingly rigid. Between $\mu = 0.1$ and $\mu = 0.8$ there is a clear transition between a state where F_μ is small compared to typical tangential forces, and slip is easy, to a state where very few particles experience sufficient tangential force to reach F_μ.

The effect that this has on the dynamics of a bubbling bed were not immediately apparent in the system shown in figure 2. Instead, the fluid inlet was changed to a jet of velocity $50\,\text{mm}\,\text{s}^{-1}$, spanning

0.9 mm in the centre of the bed. This created a more predictable bubbling pattern, with bubbles of approximately constant size propagating up the centre of the domain. The results of sampling these bubbles at a height of 3.5 mm and measuring their velocities are shown in figure 14. It is observed that the bubble velocity falls initially before rising again, approximately mirroring the relationship shown in figure 12. This result lends itself to the somewhat intuitive interpretation that bubbles in beds of Geldart A powders will propagate fastest through particles which are more loosely packed.

Conclusions

In this paper, detailed DEM simulations of fluidized beds have been performed to study the effect of particle properties on the fluidization of fine powders. Although there are multiple studies on the effect of particle size and fluid velocity of fluidized beds, there are relatively few papers concerning other particle properties – particularly in the presence of adhesive forces. One reason for the lack of knowledge in this area is the excessive computational cost involved in DEM simulations of many particles with a realistic elastic modulus. Indeed, many research papers using DEM use an excessively low value of the elastic modulus.

This study investigates the effects of varying the elastic modulus, coefficient of restitution, and coefficient of friction on the behaviour of fluidized beds of adhesive particles. The elastic modulus is of particular interest because of the frequency with which a reduced elastic modulus is used, to allow for larger simulations. In order to characterise the fluidized bed behaviour, the average particle coordination number and properties of bubbles have been calculated and discussed.

It has been shown that lowering the elastic modulus significantly changes the dynamics of a bubbling fluidized bed of adhesive particles. A lower value of E tends to lead to smaller bubbles in the presence of adhesive forces, but does not significantly effect the size bubbles in systems of non-adhesive particles. It appears that bubble velocity is largely unaffected by a change in E, however in the case of adhesive particles below a critical value bubbles cease to propagate. Investigating the pressure drop across the bed confirmed that the minimum bubbling velocity is increased for softer particles. This is attributed

to longer contact durations, and therefore more dissipation of kinetic energy over the course of a collision. It is possible that this effect could be mitigated, to some extent, by increasing the coefficient of restitution, and thereby maintaining the critical bounce velocity of a system of harder particles.

The effect of the coefficient of friction is more subtle. Up to a point, increasing the coefficient of friction increases the average particle coordination number. This is attributed to the formation of larger clusters due to the increased dissipation in the system. Beyond a value of $\mu \sim 0.2$, however, the coordination number falls again. This is thought to be because of the increasing rigidity of clusters as particles become unable to slide over one another due to the friction caused by adhesive forces. In the case of varying friction, the velocity of bubbles appears related to the coordination number, with bubbles propagating slower when particles have more contacts on average.

The insights gained in this study might be used to inform both the design and simulation of fluidized beds.

Acknowledgements

Robert Wilson was supported through a studentship in the Centre for Doctoral Training on Theory and Simulation of Materials at Imperial College London funded by the Engineering and Physical Sciences Research Council under grant number EP/G036888/1.

References

[1] Zhu H, Zhou ZY, Yang RY, Yu AB. Discrete particle simulation of particulate systems: A review of major applications and findings. *Chem Eng Sci.* 2008;63:5728–5770.

[2] Geldart D. *Gas Fluidization Technology.* Bradford: John Wiley & Sons. 1986.

[3] McKeen T, Pugsley T. Simulation and experimental validation of a freely bubbling bed of FCC catalyst. *Powder Technology.* 2003;129:139–152.

[4] Tebianian S, Dubrawski K, Ellis N, Cocco Ra, Hays R, Reddy Karri S, Leadbeater TW, Parker DJ, Chaouki J, Jafari R, Garcia-Trinanes P, Seville JP, Grace JR. Investigation of particle velocity in FCC gas-fluidized beds based on different measurement techniques. *Chemical Engineering Science*. 2015;127:310–322.

[5] Balachandar S, Eaton JK. Turbulent Dispersed Multiphase Flow. *Annual Review of Fluid Mechanics*. 2010;42(1):111–133.

[6] Curtis JS, van Wachem BGM. Modeling particle-laden flows: A research outlook. *AIChE Journal*. 2004;50(11):2638–2645.

[7] van Wachem BGM, Sasic S. Derivation, simulation and validation of a cohesive particle flow CFD model. *AIChE Journal*. 2008;54(1):9–19.

[8] Cundall PA, Strack ODL. A discrete numerical model for granular assemblies. *Géotechnique*. 1979; 29(1):47–65.

[9] Johnson K. *Contact Mechanics*. Cambridge, UK: Cambridge University Press. 2003.

[10] Hoomans B, Kuipers J, Briels W, Van Swaaij W. Discrete particle simulation of bubble and slug formation in a two-dimensional gas-fluidised bed: a hard-sphere approach. *Chemical Engineering Science*. 1996;51(1):99–118.

[11] Moreno-Atanasio R, Xu B, Ghadiri M. Computer simulation of the effect of contact stiffness and adhesion on the fluidization behaviour of powders. *Chemical Engineering Science*. 2007;62(1-2):184–194.

[12] Hou Q, Zhou Z, Yu A. Micromechanical modeling and analysis of different flow regimes in gas fluidization. *Chemical Engineering Science*. 2012;84:449–468.

[13] Kobayashi T, Tanaka T, Shimada N, Kawaguchi T. DEMCFD analysis of fluidization behavior of Geldart Group A particles using a dynamic adhesion force model. *Powder Technology*. 2013; 248:143–152.

[14] Yang F, Thornton C, Seville J. Effect of surface energy on the transition from fixed to bubbling gas-fluidised beds. *Chemical Engineering Science*. 2013;90:119–129.

[15] Tsuji Y, Tanaka T, Ishida T. Lagrangian numerical simulation of plug flow of cohesionless particles in a horizontal pipe. *Powder Technology*. 1992;71(3):239–250.

[16] Kuang SB, Chu KW, Yu AB, Zou ZS, Feng YQ. Computational Investigation of Horizontal Slug Flow in Pneumatic Conveying. *Industrial and Engineering Chemistry Research*. 2008;47(2):470–480.

[17] Hemph R, van Wachem BGM, Almstedt A. DEM modeling of hopper flows: comparison and validation of models and parameters. In: *World Conference onParticle Technology, Orlando, Florida*. 2006; .

[18] Bradley R. The cohesive force between solid surfaces and the surface energy of solids. *Philosophical Magazine*. 1932;13:853.

[19] Derjaguin B. Effect of contact deformations on the adhesion of particles. *Journal of Colloid and Interface Science*. 1975;53(2):314–326.

[20] Johnson K, Kendall K, Roberts A. Surface energy and the contact of elastic solids. *Proceedings of the Royal Society of London A Mathematical and Physical Sciences*. 1971;324(1558):301.

[21] Maugis D. Adhesion of spheres: the JKR-DMT transition using a Dugdale model. *Journal of Colloid and Interface Science*. 1992;150(1):243 – 269.

[22] Greenwood Ja. Adhesion of elastic spheres. *Proceedings of the Royal Society A: Mathematical, Physical and Engineering Sciences*. 1997;453(1961):1277–1297.

[23] Tabor D. Surface forces and surface interactions. *Journal of Colloid and Interface Science*. 1977; 58(1):2–13.

[24] Muller V, Derjaguin B, Toporov Y. On two methods of calculation of the force of sticking of an elastic sphere to a rigid plane. *Colloids and Surfaces*. 1983;7:251–259.

[25] Rabinovich Y, Adler J, Ata A, Singh R, Moudgil B. Adhesion between Nanoscale Rough Surfaces 2. *Journal of colloid and interface science*. 2000;232:17–24.

[26] Medina S, Dini D. A numerical model for the deterministic analysis of adhesive rough contacts down to the nano-scale. *International Journal of Solids and Structures*. 2014;51:2620–2632.

[27] Jones R, Pollock H, Geldart D, Verlinden a. Inter-particle forces in cohesive powders studied by AFM: effects of relative humidity, particle size and wall adhesion. *Powder Technology*. 2003;132(2-3):196–210.

[28] Ecke S, Butt HJ. Friction between Individual Microcontacts. *Journal of Colloid and Interface Science*. 2001;244:432–435.

[29] Mindlin RD, Deresiewicz H. Elastic spheres in contact under varying oblique forces. *J of Appl Mech*. 1953;20:327–344.

[30] Maxey MR, Riley JRJ. Equation of motion for a small rigid sphere in a nonuniform flow. *Physics of Fluids*. 1983;26(4):883.

[31] Wen C, Yu Y. Mechanics of fluidization. *Chem Eng Prog Symp Ser*. 1965;62(62):100–111.

[32] Gidaspow D. *Multiphase Flow and Fluidization*. San Diego: Academic Press. 1994.

[33] Ergun S. Fluid flow through packed columns. *Chem ENG Prog*. 1952;48:89–94.

[34] van Wachem B, Schouten J, van den Bleek C, Krishna R, Sinclair J. Comparative Analysis of CFD Models of Dense Gas Solid Systems. *AIChE Journal*. 2001;47(5).

[35] Jackson R. Locally averaged equations of motion for a mixture of identical spherical particles and a Newtonian fluid. *Chemical engineering science*. 1997;52(15):2457–2469.

[36] Sanchez-Valle C, Sinogeikin SV, Lethbridge ZaD, Walton RI, Smith CW, Evans KE, Bass JD. Brillouin scattering study on the single-crystal elastic properties of natrolite and analcime zeolites. *Journal of Applied Physics*. 2005;98(5):053508.

[37] Feng Y, Yu A. Effect of bed thickness on the segregation behavior of particle mixtures in a gas fluidized bed. *Industrial & Engineering Chemistry Research*. 2010;49:3459–3468.

[38] Cammarata L, Lettieri P, Micale GDM, Colman D. 2D and 3D CFD Simulations of Bubbling Fluidized Beds Using Eulerian-Eulerian Models. *International Journal of Chemical Reactor Engineering*. 2003;1.

[39] Tsuji Y, Kawaguchi T, Tanaka T. Discrete particle simulation of two-dimensional fluidized bed. *Powder Technology*. 1993;77(1):79–87.

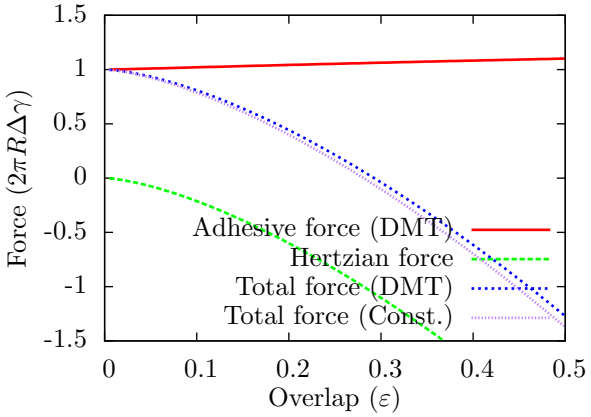

Figure 1: The contact force in the DMT model compared to a constant adhesive force for particles with a Tabor parameter of $\mu = 0.1$

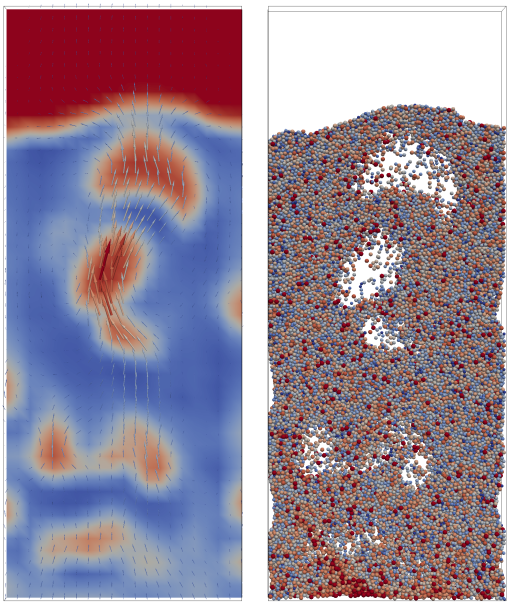

Figure 2: The simulated fluidized bed. Fluid volume fraction and velocity are shown on the left, and individual particles on the right. Particles are colour coded by size from 47.6 µm (dark blue) to 72.4 µm (dark red).

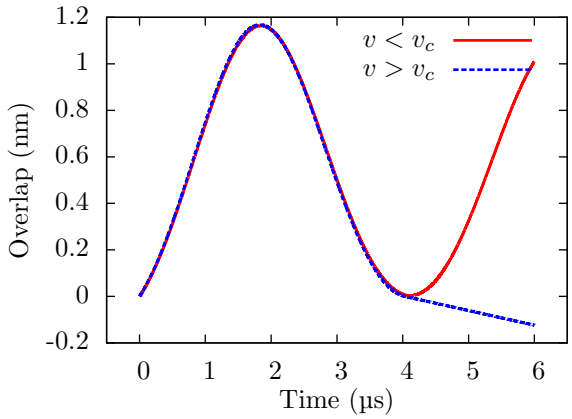

Figure 3: Contact overlap for collisions with incident velocity $v < v_c$ and $v > v_c$.

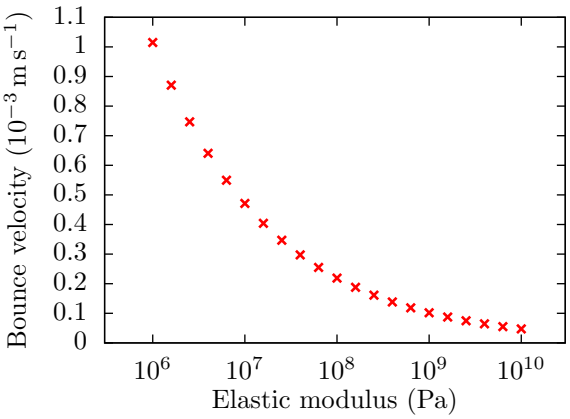

Figure 4: The critical velocity required for two particles to bounce for a range of elastic moduli.

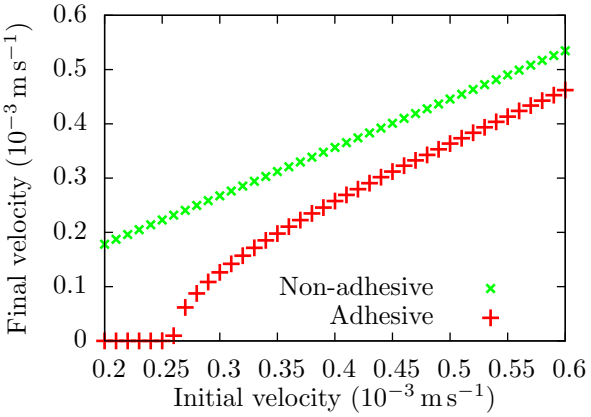

Figure 5: A comparison of initial and final velocities for adhesive and non-adhesive particles.

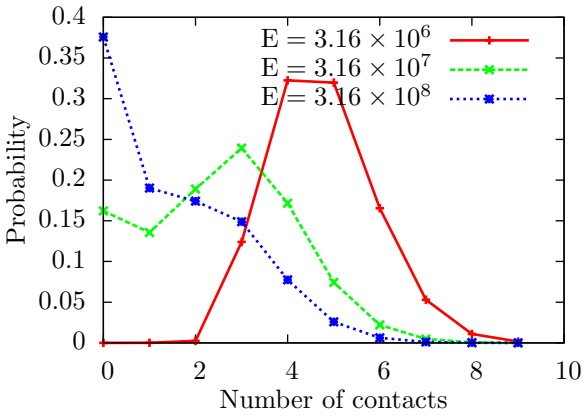

(a) Probability distribution of coordination numbers for adhesive particles at three elastic moduli.

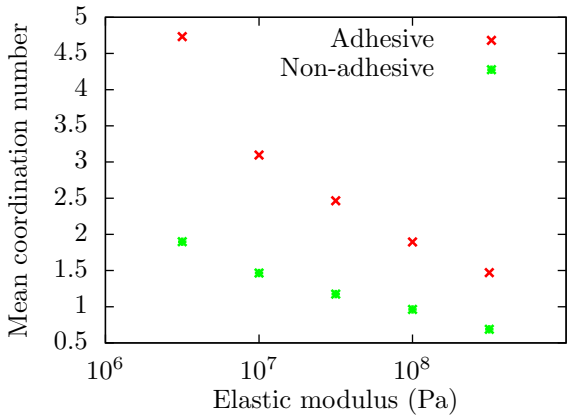

(b) Average coordination number as a function of elastic modulus for adhesive and non-adhesive particles.

Figure 6: Coordination number probability distribution and average values for a range of elastic moduli.

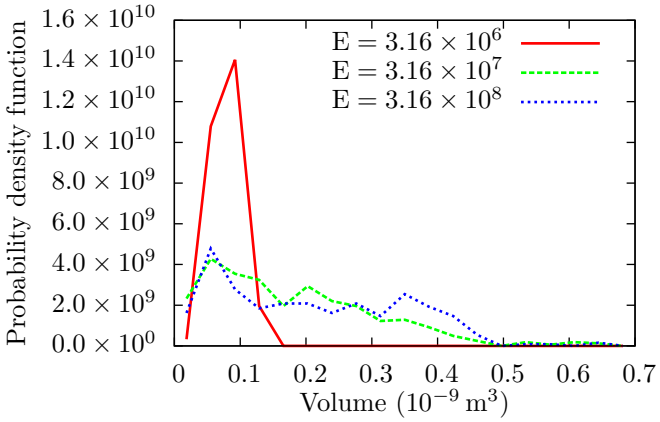

(a) PDF of bubble volumes for adhesive particles at three elastic moduli.

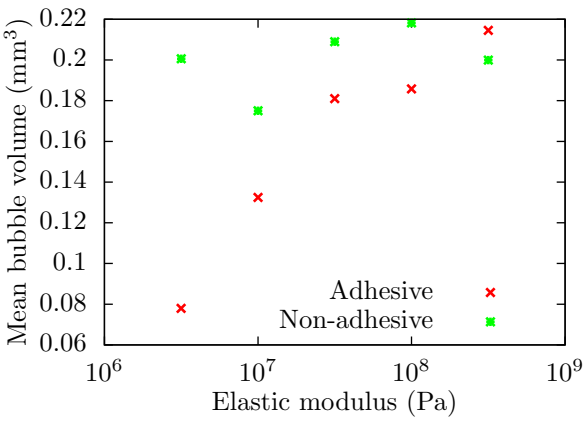

(b) Average bubble volume as a function of elastic modulus for adhesive and non-adhesive particles.

Figure 7: Averages and probability distribution functions (PDFs) of bubble volumes for a range of elastic moduli.

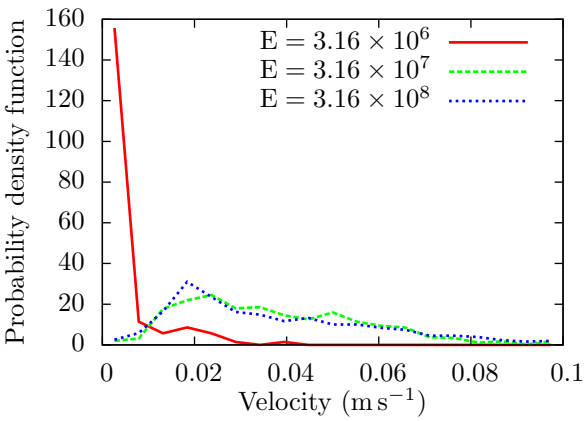

(a) PDF of bubble velocities for adhesive particles of three elastic moduli.

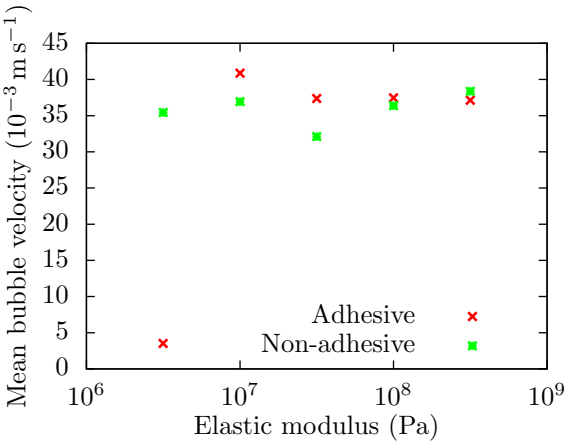

(b) Average bubble velocity as a function of elastic modulus for adhesive and non-adhesive particles.

Figure 8: Averages and PDFs of bubble velocities for a range of elastic moduli.

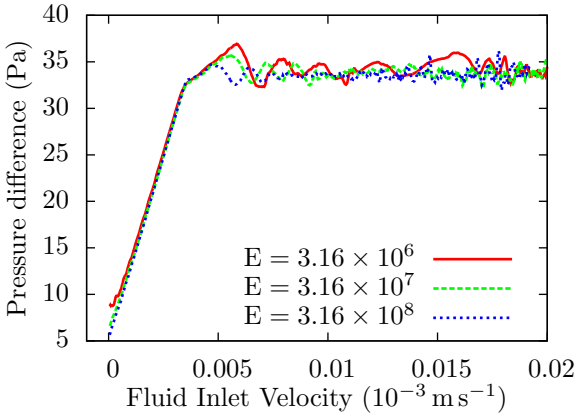

Figure 9: Pressure as a function of fluid inlet velocity for particles with a number of elastic moduli.

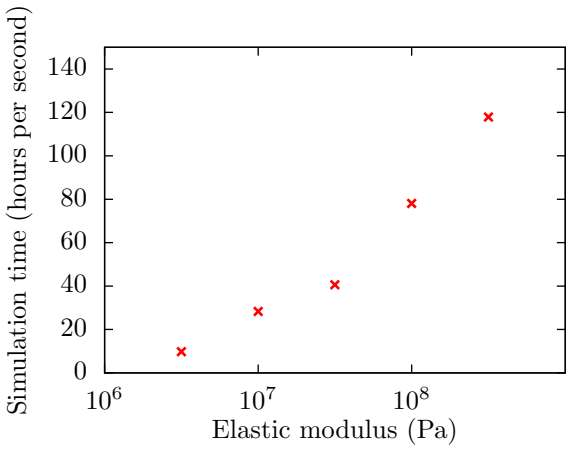

Figure 10: Time taken to run 1 s of a simulation for each of the elastic moduli investigated.

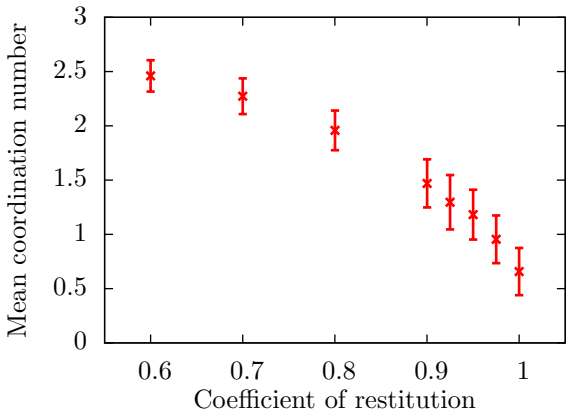

Figure 11: Average coordination number as a function of coefficient of restitution. Error bars represent the variation in this average over the course of a simulation. Properties other than the coefficient of restitution take the values given in table 1.

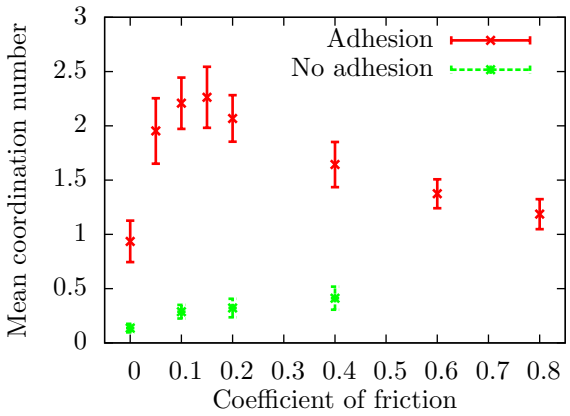

Figure 12: Average coordination number as a function of coefficient of friction for adhesive and non-adhesive particles. Error bars represent the variation in this average over the course of a simulation.

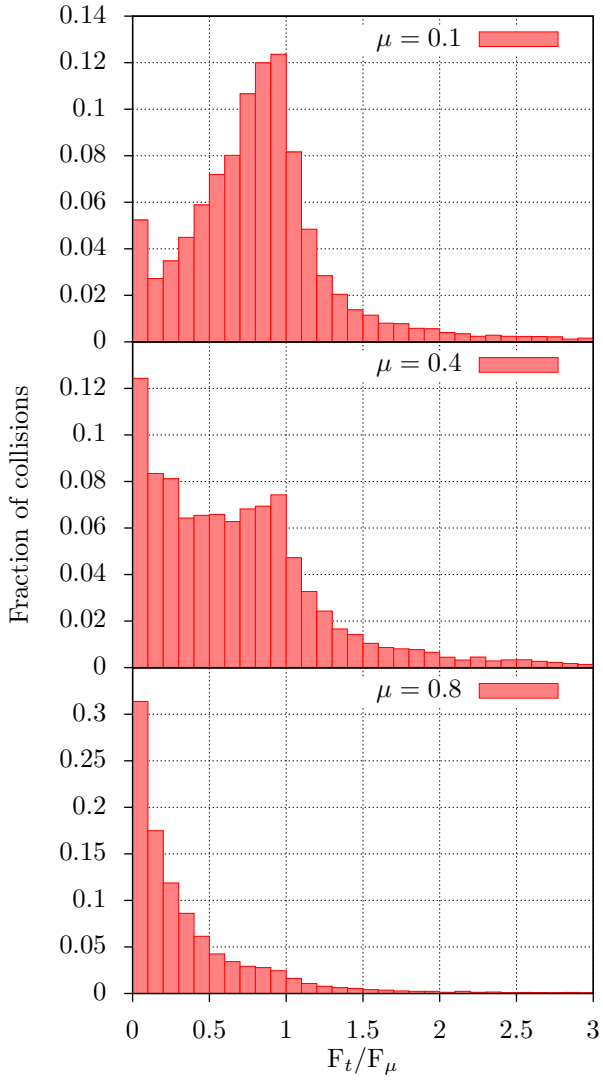

Figure 13: Probability density of particles experiencing a given tangential force. Units are the critical tangential force required for slip.

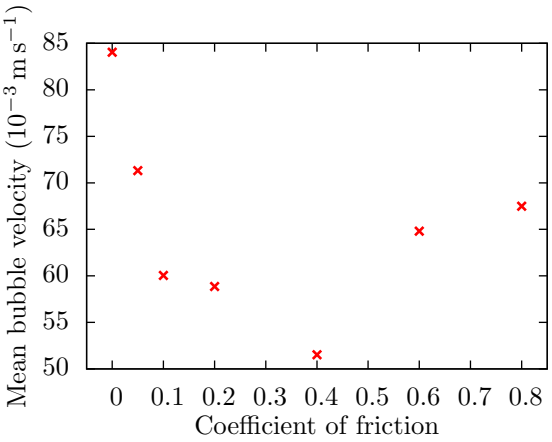

Figure 14: Bubble velocity at a height of 3.5 mm for a fluidized bed with a central jet of velocity 50 mm s^{-1}

Particle properties	
Diameter, d	Gaussian: $\mu = 60\,\mu\text{m}$ $\sigma = 6\,\mu\text{m}$
Density, ρ	$2200\,\text{kg}\,\text{m}^{-3}$
Elastic modulus, E	$3.162 \times 10^{7}\,\text{Pa}$
Poisson ratio, ν	0.33
Coeff. friction, μ	0.35
Coeff. restitution, e	0.85
Work of adhesion, $\Delta\gamma$	5×10^{-5}
Equilibrium distance, ε	5×10^{-10}
Domain properties	
Dimensions	$\text{L}_z = 0.36\,\text{mm}$ (2 cells) $\text{L}_y = 3.6\,\text{mm}$ (20 cells) $\text{L}_x = 9\,\text{mm}$ (50 cells)
Inlet velocity	$0.02\,\text{m}\,\text{s}^{-1}$
Number of particles	34 952
Fluid properties	
Density	$0.7118\,\text{kg}\,\text{m}^{-3}$
Viscosity	$25.04 \times 10^{-6}\,\text{Pa}\,\text{s}$

Table 1: The physical parameters used in fluidization simulations.